Geochemistry Geophysics Geosystems G3
AN ELECTRONIC JOURNAL OF THE EARTH SCIENCES
Published by AGU and the Geochemical Society

Article
Volume 8, Number 2
14 February 2007
Q02007, doi:10.1029/2006GC001394
ISSN: 1525-2027

Click Here for Full Article

Biogenic nitrogen and carbon in Fe-Mn-oxyhydroxides from an Archean chert, Marble Bar, Western Australia

Daniele L. Pinti
GEOTOP-UQÀM-McGill and Département des Sciences de la Terre et de l'Atmosphère, Université du Québec à Montréal, Montreal, Quebec, Canada H2X 3Y7 (pinti.daniele@uqam.ca)

Ko Hashizume
Department of Earth and Space Sciences, Graduate School of Science, Osaka University, Toyonaka, Osaka 560-0043, Japan

Beate Orberger
Université Paris XI SUD, UMR IDES-8148 (UPS-CNRS), Département des Sciences de la Terre, Bat. 509, F-91405 Orsay Cedex, France

Jean-Paul Gallien
Laboratoire Pierre Süe, CEA-CNRS, UMR 9956, CEA Saclay, F-91191 Gif-sur-Yvette Cedex, France

Christophe Cloquet
GEOTOP-UQÀM-McGill and Département des Sciences de la Terre et de l'Atmosphère, Université du Québec à Montréal, Montreal, Quebec, Canada H2X 3Y7

Now at Department of Analytical Chemistry, INW-UGent, Proeftuinstraat 86, 9000 Ghent, Belgium

Marc Massault
Université Paris XI SUD, UMR IDES-8148 (UPS-CNRS), Département des Sciences de la Terre, Bat. 509, F-91405 Orsay Cedex, France

[1] To quantify and localize nitrogen (N) and carbon (C) in Archean rocks from the Marble Bar formation, Western Australia, and to gain insights on their origin and potential biogenicity, we conducted nuclear reaction analyses (NRA) and carbon and nitrogen isotope ratio measurements on various samples from the 3460-Myr-old Fe-rich Marble Bar chert. The Marble Bar chert formed during the alteration of basaltic volcanoclastic rocks with Fe- and Si-rich hydrothermal fluids, and the subsequent precipitation of magnetite, carbonates, massive silica, and, locally, sulfides. At a later stage, the magnetite, sulfides, and carbonates were replaced by Fe-Mn-oxyhydroxides. Nuclear reaction analyses indicate that most of the N and C resides within these Fe-Mn-oxyhydroxides, but a minor fraction is found in K-feldspars and Ba-mica dispersed in the silica matrix. The N and C isotopic composition of Fe-oxides suggests the presence of a unique biogenic source with $\delta^{15}N_{AIR}$ values from +6.0 ± 0.5‰ to 7.3 ± 1.1‰ and a $\delta^{13}C_{PDB}$ value of −19.9 ± 0.1‰. The C and N isotope ratios are similar to those observed in Proterozoic and Phanerozoic organic matter. Diffusion-controlled fractionation of N and C released during high combustion temperatures indicates that these two elements are firmly embedded within the iron oxides, with activation energies of 18.7 ± 3.7 kJ/mol for N and 13.0 ± 3.8 kJ/mol for C. We propose that N and C were chemisorbed on iron and were subsequently embedded in the crystals during iron oxidation and crystal growth. The Fe-isotopic composition of the Marble Bar chert ($\delta^{56}Fe = -0.38 \pm 0.02$‰) is similar to that measured in iron oxides formed by direct precipitation of iron from hydrothermal plumes in contact

with oxygenated waters. To explain the N and C isotopic composition of Marble Bar chert, we propose either (1) a later addition of N and C at the end of Archean when oxygen started to rise or (2) an earlier development of localized oxygenated environments, where biogeochemical cycles similar to modern ones could have developed.

Components: 10,993 words, 9 figures, 2 tables.

Keywords: nitrogen isotopes; carbon isotopes; iron isotopes; Archean; Marble Bar chert; biosignatures.

Index Terms: 1041 Geochemistry: Stable isotope geochemistry (0454, 4870); 1055 Geochemistry: Organic and biogenic geochemistry; 5215 Planetary Sciences: Astrobiology: Origin of life; 5225 Planetary Sciences: Astrobiology: Early environment of Earth.

Received 21 June 2006; **Revised** 7 November 2006; **Accepted** 20 November 2006; **Published** 14 February 2007.

Pinti, D. L., K. Hashizume, B. Orberger, J.-P. Gallien, C. Cloquet, and M. Massault (2007), Biogenic nitrogen and carbon in Fe-Mn-oxyhydroxides from an Archean chert, Marble Bar, Western Australia, *Geochem. Geophys. Geosyst.*, *8*, Q02007, doi:10.1029/2006GC001394.

1. Introduction

[2] A significant portion of nitrogen (N) in sedimentary rocks is of biological origin, mainly occurring as ammonium (NH_4^+) [*Boyd*, 2001]. Ammonium can be found as (1) exchangeable NH_4^+ representing organic nitrogen that has been decomposed in sediments most recently or (2) fixed NH_4^+ derived from the decomposition of organic substances during diagenesis. In the first form, NH_4^+ is adsorbed on clay surfaces, while as fixed NH_4^+, it is bound to the lattice of mica and feldspars minerals, replacing K^+ ions [*Honma and Itihara*, 1981]. The $^{15}N/^{14}N$ ratio (expressed as $\delta^{15}N$) of the fixed NH_4^+ is mainly constrained by the N-isotopic composition of the organic nitrogen prior to diagenesis. Thus $\delta^{15}N$ of lattice-bound, or diagenetic, NH_4^+ has the potential to function as a paleoindicator [*Shen et al.*, 2006].

[3] Compared to other bioindicative elements such as (organic) carbon or sulfur, nitrogen is characterized by its non-reactive chemical behavior and its high volatility. The first characteristic, largely owing to the exceeding stability of N_2 molecules, which strictly limits inorganic transmission of N from the atmosphere to the biosphere via *atmospheric N fixation*, may lead to construction of a simpler biological flux model of N from the atmosphere to the sediment [*Shen et al.*, 2006]. The latter suggests that N isotopic information in old sedimentary rocks can be biased by various post-sedimentary geological events [*Boyd and Philippot*, 1998; *Dauphas and Marty*, 2004]. A correct interpretation of the Precambrian nitrogen $^{15}N/^{14}N$ isotopic ratio in terms of biogenesis requires (1) detection of the mineral or organic sites where N resides; (2) assessment of the speciation of N; and (3) knowledge of the post-depositional events potentially affecting N-hosting minerals.

[4] Recent studies on Precambrian sediments [*Boyd and Philippot*, 1998; *Beaumont and Robert*, 1999; *Pinti et al.*, 2001; *Jia and Kerrich*, 2004; *van Zuilen et al.*, 2005; *Papineau et al.*, 2005; *Ueno et al.*, 2004; *Nishizawa et al.*, 2005; *Shen et al.*, 2006] showed the high potential of N as a biomarker. Yet, they also showed its limitations which are mainly due to our poor understanding of the origin of N in sediments and of the geochemical behavior of nitrogen during early diagenesis [*Freudenthal et al.*, 2001; *Lehmann et al.*, 2002] weathering [*Busigny et al.*, 2005] and metamorphism [*Busigny et al.*, 2003].

[5] Most studies of the Precambrian nitrogen cycle have been focused on cherts. The Precambrian cherts have often been considered as chemical precipitates from a warm and silica-saturated Archean ocean [*Siever*, 1992]. However, an increasing number of studies have provided evidence that the cherts are, in fact, "replacement cherts," that is, sediments (often volcanoclastic) that have been post-depositionally silicified by pervasive hydrothermal or diagenetic fluids [*de Wit et al.*, 1982; *Paris et al.*, 1985; *Sugitani*, 1992; *Kato and Nakamura*, 2003; *Hofmann*, 2005; *Orberger et al.*, 2006c; see also *Perry and Lefticariu*, 2003]. Post-depositional alteration [*Rouchon et al.*, 2004], and metamorphism [*Boyd and Philippot*, 1998] of these cherts can also alter their primary

biogenic N (and C) isotopic signature [*Dauphas and Marty*, 2004; *Pinti et al.*, 2001].

[6] Ammonium in mica is not the only form of N in ancient rocks [*Honma*, 1996; *Rouchon et al.*, 2005; *Papineau et al.*, 2005; *Boyd and Philippot*, 1998]. *Sano and Pillinger* [1990] suggested the occurrence of N_2 in fluid inclusions and *de Ronde et al.* [1997] found ammonium or ammonia in hydrothermal fluid inclusions in Archean ironstones of South Africa. *Pinti et al.* [2001] and, more recently, *Nishizawa et al.* [2005] have shown that magnetite from banded iron formations (BIFs) contain significant amounts of N in unknown form [*Shen et al.*, 2006; *Cloquet et al.*, 2006]. Recent data by *Orberger et al.* [2005, 2006c] indicate that biogenic apatite and sulfides host significant amounts of organic C and N in Paleozoic black shales.

[7] The objective of this study is to investigate in detail the sources and fate of nitrogen and carbon in a Precambrian chert using quantitative micrometric and nanometric scale in situ analyses of N and C by nuclear reaction analysis (NRA hereafter) [*Gallien et al.*, 2004; *Rouchon et al.*, 2005; *Orberger et al.*, 2005] combined with stepped-combustion extraction and isotopic analysis of N by mass spectrometry [*Yamamoto et al.*, 1998; *Pinti et al.*, 2001]. We focus on the search of geochemical and isotopic "fingerprints," providing signs of ancient life. The studied sample is an Eoarchean chert (A458) from the Pilbara Craton, Western Australia. It is composed of (1) a replacement chert, representing a silicified basaltic rock; (2) iron oxide bands alternating with silica bands with a stromatolitic texture; and (3) a pure chert precipitate.

2. The 3.5 Ga Chert A458 From Marble Bar–Towers Formation

[8] The Marble Bar chert sample A458 (Australian Map Grid 50, 782100mE, 7654600mN; Geographical 21°11′17.3760″ lat, 119°43′1.2397″ long) belongs to the A-section of the Towers Formation (Figure 1a), a 45 m-thick sequence of ferruginous cherts directly overlying Fe-rich, K-poor, MOR-like tholeiitic basalts in Marble Bar, Western Australia (Figure 1b) [*Kato and Nakamura*, 2003]. The estimated depositional age of the Marble Bar Chert Unit is between 3474 and 3433 Ma [*Thorpe et al.*, 1992]. These cherts have been interpreted as precipitates from a high-temperature Fe- and Si-rich hydrothermal solution emanating from a Mid Ocean Ridge [*Kato and Nakamura*, 2003].

[9] *Orberger et al.* [2006b] provide a detailed mineralogical and geochemical description of the sample. In brief, the sample A458 is a composite chert consisting of a dark gray part (zone I), a microbanded iron layer a few millimeters thick (zone II), and a light gray part (zone III, Figure 2a). Prior to silicification, the precursor rock of zone I had a porphyritic or porphyroclastic texture, typical of volcaniclastic rocks. Precursor minerals were most likely pyroxenes, amphiboles and feldspars, suggesting a basaltic protolith (Figure 2c) [*Orberger et al.*, 2006b]. The presence of euhedral Fe-sulfides point to a reducing environment during silicification (Figure 2c). Zone II is composed of alternating, millimeter-size iron-manganese oxyhydroxide (named FeMnOH hereafter) and quartz bands with a stromatolitic texture (Figure 2b). The iron bands are formed of skeletal goethite aggregates and euhedral rhombic-shaped phenocrysts of FeMnOH. The phenocrysts have an inner euhedral core with a vermicular texture and a heterogeneous composition reflected by bright and dark microbands under scanning electron microprobe (Figure 2e). A euhedral filamentous overgrowth zone is separated from the inner crystal by K-Al silicates, possibly illite (Figure 2e). Magnetite inclusions in the silica bands intercalated with the FeMnOH bands (Figure 2d) indicate that these layers were originally composed of magnetite and Ca-Mg-carbonates.

[10] Focused Ion Beam-Transmission Electron Microscope (FIB–TEM) investigations at the GFZ-Potsdam showed that each microband of FeMnOH is composed of nanometric filaments, each of them consisting of euhedral hematite crystals with an average size of 100 nm [*Orberger et al.*, 2006a, 2006b]. The vermicular microscopic textures and filamentous, clustered nanotextures of the hematite can possibly be related to microbial activity. Similar nanotextures were observed in ferrihydrite formed by the activity of Fe-oxidizing bacteria growing in near-neutral pH groundwater [*Banfield and Zhang*, 2001]. Electron microprobe analyses showed that the FeMnOH phenocrysts contain traces of Ca and Mg, which were left from precursor carbonates. Zone III represents a chert precipitate composed of microcrystalline quartz, intergrown with micrometric K-Al-silicates (Figure 2f), and, occasionally, barite, Ba-rich mica and/or Fe-sulfides. The latter have a texture similar to the FeMnOH

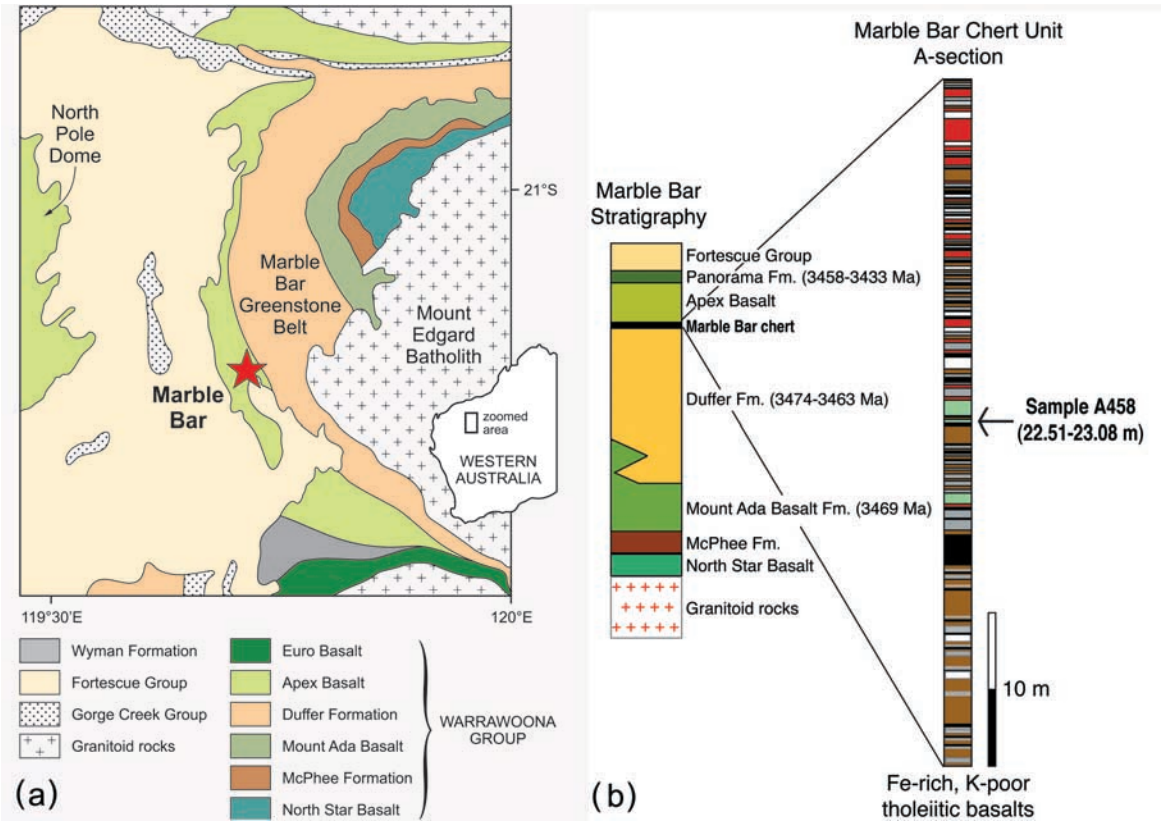

Figure 1. (a) Localization of the Marble Bar Pool chert formation at Pilbara craton, Western Australia, and (b) a simplified stratigraphic column. Figure 1a simplified from that of *Van Kranendonk et al.* [2001]; Figure 1b redrawn and simplified from that of *Kato and Nakamura* [2003] with permission from Elsevier.

bands. The chert is cut by millimeter-scale quartz veins, also containing FeMnOH, with textures similar to those observed in the main FeMnOH bands (Figures 2a and 2b).

[11] *Orberger et al.* [2006b] proposed a model of the chert formation, in which the Fe-microbands were initially composed of magnetite, Ca-Mg-carbonates and sulfides, precipitated from a reducing, hot ($\geq$250°C), hydrothermal fluid. Subsequently, oxidizing fluids infiltrated the chert along selective permeable zones such as the magnetite-carbonate layer (zone II) and the crosscutting quartz veins (zone III). During this episode, magnetite was oxidized to FeMnOH and carbonates were dissolved, and, replaced by FeMnOH.

3. Analytical Techniques

3.1. NRA Analytical Procedure for N and C Determinations

[12] The CEA-CNRS Pierre Süe Laboratory nuclear microprobe [*Khodja et al.*, 2001] was used to achieve in situ N and C determination in chert A458. The analysis chamber allows performing simultaneously measurements of the light element abundances (^{12}C, ^{14}N, ^{16}O, ^{28}Si, ^{27}Al and ^{32}S) by Nuclear Reaction Analysis, as well as the determination of heavier element abundances such as Ni, Fe, Zn, Ca and K by X-ray [*Mosbah et al.*, 1993; *Gallien et al.*, 2004]. A 1.9 MeV deuteron ($^{2}H^{+}$) incident beam was used to achieve the maximum sensitivity for nitrogen detection. The ^{14}N(d, p_0)^{15}N and ^{12}C(d, p_0)^{13}C nuclear reactions are used to quantify N and C, respectively. The deuteron beam is focused to 3 $\times$ 3 μm^2 whose intensity is close to 0.8 nA. Nuclear reaction light product were detected using a 130 mSr, 1500 μm depletion depth annular silicon surface barrier detector located at 170°. X-rays were measured using a 95 μm^2, collimated high-purity germanium detector with a 50 μm Mylar filter to stop most charged particles. Backscattered particles are stopped in the Mylar screen, but higher energy charged particles derived from nuclear reactions can pass. These analytical conditions led to a counting rate of few hundred particles per seconds, depending on the mineral composition.

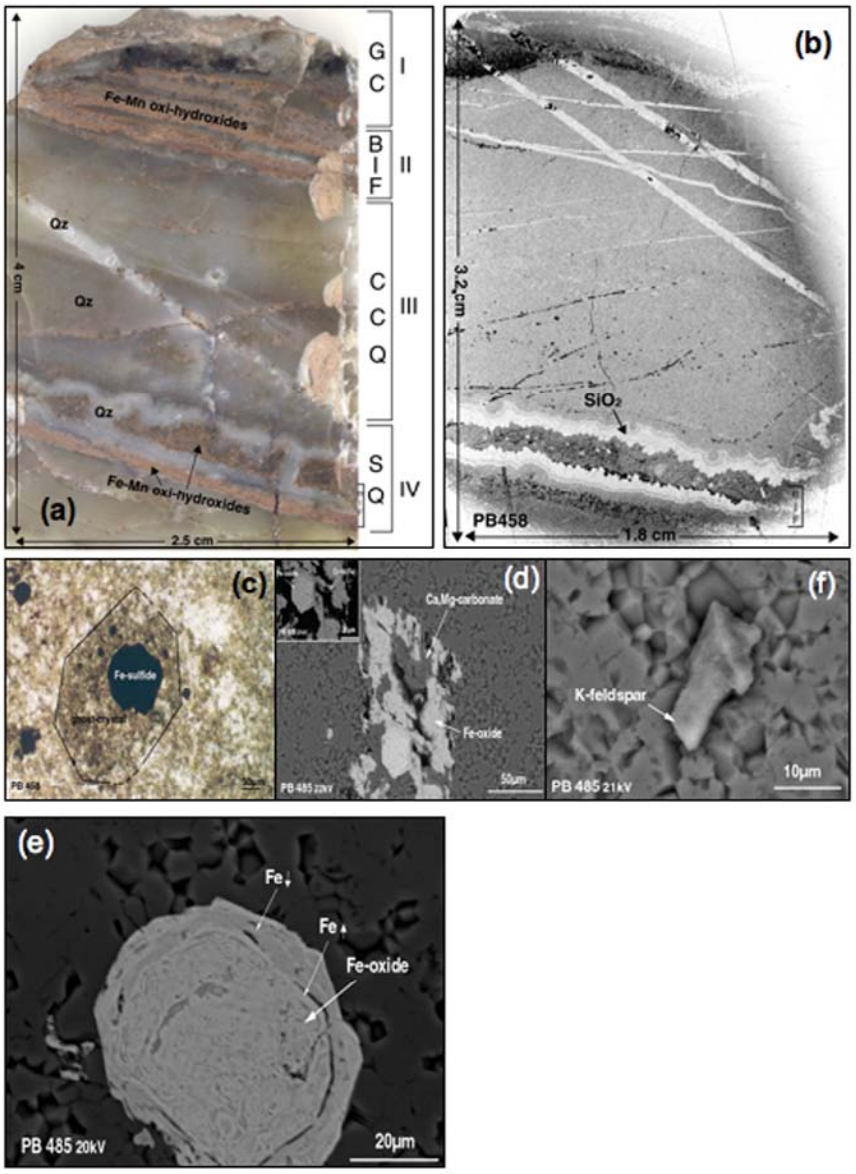

Figure 2. (a) Polished section scan of the sample A458 studied here. The two iron oxide microbanded layers are clearly visible. (b) Polished thin section scan macrophotograph of the sample A458 showing the stromatolite-like structure of the iron oxide bands alternating with quartz bands (Zone II). (c) Transmitted not polarized optical microscopic photograph of a precursor mineral (possibly pyroxene), now composed of microcrystalline quartz. Euhedral Fe-sulfide crystals are precipitated preferentially in these precursor relicts (Zone I).(d) SEM-BSE image: Ca-Mg carbonate replaced by FeMnOH (zone II). (e) Scanning electron microscope-backscattered electron (SEM-BSE) image: euhedral FeMnOH, with internal vermicular structure of heterogeneous chemical composition. The interface between the overgrowth and the internal euhedral crystal is composed of K-Al silicate, possibly illite (zone II). (f) SEM-BSE image: subhedral orthoclase intergrown in the cryptocrystalline quartz matrix of zone III.

[13] A subsample ($4 \times 2.5 \times 0.5$ cm^3) was cut (Figure 2a), polished with aluminum oxide powder, cleaned in an ultrasonic bath and coated with gold, to avoid contamination. Signals only from 1 to ~9 μm depth were used for N and C quantification. The first micron was discarded to avoid surface contamination. Point analyses were performed on K-Al silicates, sulfides and quartz, while scanning mode was used for highly heterogeneous FeMnOH in order to select the most suitable (in terms of size and thickness) area for N and C determination. The MPAWIN data acquisition software was run in the "listcard-coincident" mode and the generated data files were processed with the homemade RISMIN

Table 1. C and N Elemental Analyses Done by NRA on Chert Sample A458[a]

Sample Number	Mineral Phases	C, at. %	N, at. %	C, eq. ppm	N, eq. ppm	C/N, atomic
		Scans (100 × 100 μm²)				
PB4581f max	Fe-Mn oxide bands	1.59	0.51	6049	2241	3.1
PB4581f min		0.80	0.11	3010	497	7.0
PB4581l max	Fe-Mn oxide bands	1.98	0.35	7550	1549	5.6
PB4581l min		0.91	0.05	3437	206	19.3
PB4581m max	Fe-Mn oxide bands	1.14	0.24	4306	1065	4.7
PB4581m min		0.91	0.08	3439	355	11.3
PB4581g max	Fe-Mn oxide bands	1.35	0.12	5108	525	11.3
PB4581g min		1.05	0.45	3983	1973	2.3
		Micro-scans (20 × 20 μm²)				
PB4581gB max	microscan of PB458g	1.26	0.22	4786	985	5.6
PB4581gB min		0.75	0.11	2833	492	6.7
S8-458-Fe	Fe oxide	4.00	0.08	15436	333	52.8
S8-458-Qz	Quartz around Fe oxide	1.03	0.01	6203	79	91.2
		Spots (5 × 5 μm²)				
PB458803	Fe oxide	0.50	0.03	1902	113	19.5
PB4581103	Fe oxide	0.66	0.03	2474	150	19.1
PB458603	Fe-Mn oxide	0.57	0.02	2140	107	23.1
PB458403	K-Al-silicates	0.30	0.10	1792	711	2.9
PB458503	K-Al-silicates	0.70	0.25	4189	1778	2.7

[a] The C and N values for Fe-Mn-oxides have been calculated using a Fe_2O_3 matrix [*Gallien et al.*, 2004]. Calculations based on a FeO(OH) basis increase the C, N amounts of 10%. Maximum and minimum values in scans give the variation of concentration with the penetration depth. Nitrogen in sulfides of porphyric zone I, cryptocrystalline quartz of zone III, near quartz veins and in quartz from vein filling of zone IV are lower than detection limits. Carbon amount in quartz has been estimated to be 0.04 at%.

software [*Daudin et al.*, 2003]. Special care is taken to extract data (X-ray and NRA spectra) corresponding to a homogeneous phase, to correct for matrix effects.

[14] When performing NRA analyses on minerals, the spectrum is the sum of several (d, p) or (d, α) nuclear reactions (fundamental and excited states) for all "light" elements ($Z < 17$, isotopes included). With respect to our analytical conditions (beam energy, detection angle), the lack of NRA cross-section data for the contributing isotopes the following standards must be used for quantification: Al_2O_3, SiO_2, Mg, FeS_2, UO_2, $CaPO_4(OH)_5$, TiN and $CaCO_3$. The overall spectrum is fitted and backgrounds are determined especially for C measurements. The numbers of counts extracted from a defined region of NRA spectrum (related to a specific nuclear reaction) is linearly correlated to the concentration of the element analyzed and the accumulated charge. Quantification can be achieved by taking into account the matrix effect, in both the standard and the sample. The "matrix effect" in ion beam analyses (in this case NRA) is caused by the slowing-down of the particles through the matter [*Khodja et al.*, 2001]. This effect can be quantified if the composition of the standard and of the sample is well known, which is the case [*Orberger et al.*, 2006b].

[15] Analyses were done on larger scanned areas of approximately 100 × 100 μm^2 but generally 10% to 70% of the spectral data is retained, corresponding to homogeneous mineral phases. The totality of the analyzed spectrum is retained for the smaller scans of 20 × 20 μm^2 and 5 × 5 μm^2 spots (Table 1). During a few hours measurement, beam current fluctuation effects on scanned areas are minimized using a high scanning rate (1 kHz). Quantitative N microanalysis requires high a microbeam current (800 pA, 5 × 5 μm^2) to reach 20 pC-accumulated charge in a realistic time (7 hours). The detection limit of N and C by NRA is about 100 ppm.

3.2. Mass Spectrometric Techniques for Nitrogen Isotope Determinations

[16] Following NRA measurements, N and Ar isotopic abundances, and C and H_2O elemental abundances in mineral phases containing N and C (mainly FeMnOH; see Results), were measured at the Department of Earth and Space Sciences of Osaka University. An iron-rich portion of A458 was crushed to about 1-10 μm-size grains and iron-bearing particles separated by a heavy liquid (ρ = 2.66 g/cm^3), sodium polytungstate (SPT). The red-colored portion with density higher than 2.66 g/cm^3 was used in this study hereafter (referred to as A458

iron-rich separate). The iron-rich separate was washed with 60°C ultrapure water for two days in order to totally dissolve the residual SPT on the grain surfaces. The washing procedure is critical to obtain reliable data, since SPT contains significant amounts of nitrogen enriched in ^{15}N ($\delta^{15}N \geq 20‰$). Complete removal of the SPT by the current washing procedure was verified by measuring N of an industrially produced silica powder essentially free of nitrogen, which was treated by the SPT following exactly the same procedures with the samples. Prior to the N isotope analyses, the separated powder was loaded directly (without polishing and electro-conductive coating) on a low-vacuum type SEM-EDX (JSM-5510LV + JED-2300, JEOL). Major elements were determined by scanning a broad area (~1 mm^2). Major element oxide abundances are: Fe_2O_3 (54 wt.%); SiO_2 (43 wt.%); MnO (1.5 wt.%); MgO (0.8 wt.%); Al_2O_3 (0.4 wt.%); CaO (0.07 wt.%); K_2O (0.05 wt.%). Finally, after repeated washing with acetone and ethanol, a 5.86 mg aliquot of the dried sample wrapped in an annealed platinum foil was loaded into the mass spectrometry system.

[17] The mass spectrometry system includes a quadrupole mass spectrometer (QMG-420, Balzers®) with an inlet system consisting of an all-metal vacuum line to extract nitrogen from the sample, loaded in a double-walled quartz glass tube, by step combustion. *Yamamoto et al.* [1998] and *Pinti et al.* [2001] described in detail the analytical infrastructure; thus only recent improvements of the system are described below. Condensable impurities (e.g., hydrocarbons, H_2O and CO_2) were removed from the sample gas using a liquid nitrogen trap, consisting in a capillary tube made of Pyrex glass. Tests using 40 picomole (about 10^{-6} Torr) of atmospheric standard air N_2 showed that several% of the N_2 was adsorbed onto the Pyrex tube's wall. Isotopic ratios of the standard air N_2 correlated well with degree of adsorption, suggesting isotopic fractionation during adsorption, with ^{15}N enrichment in the adsorbed fraction. Interestingly, the degree of N_2 adsorption was dependent on the thickness of the glass tube, possibly through its minute effect on the temperature gradient between the inner and outer surface of the tube. Adsorption of N_2 has been avoided by using a new double-walled tube, where dry N_2 gas of an atmospheric pressure was encapsulated between the inner and outer tubes, a slight modification of the earlier method that significantly improved the quality of our N isotopic measurements.

[18] The reproducibility of nitrogen isotopic measurements, estimated through the repeated (n = 42) analysis of the standard gas over the period of a month, is 0.9‰ (1σ), which now seems to be limited by uncertainties in the reduction of hydrocarbons (C_2H_x) and subsequent isobaric interferences at m/z ratios of 28 and 29 [*Hashizume and Sugiura*, 1990]. The reproducibility for $^{40}Ar/^{36}Ar$ ratios measured in the same standard air was 1.0% (1σ). The blanks of N_2 and Ar, determined by performing the extraction and purification procedures without any sample, were typically 1–2 picomoles (N_2) and 5–20 femtomoles (^{40}Ar) at a combustion temperature of 1000°C. The N isotopic ratio ($^{15}N/^{14}N$) is expressed in the conventional delta notation, which is defined as follows: $\delta^{15}N \equiv \{[(^{15}N/^{14}N)_{sample}/(^{15}N/^{14}N)_{air}] - 1\} \cdot 1000)$, where $(^{15}N/^{14}N)_{air} = 3.653 \times 10^{-3}$.

[19] Amounts of carbon and hydrogen, converted to CO_2 and H_2O, were quantified by a pressure gauge (crystal gauge M-320XG, ANELVA), followed by examination of the gas species by a gas chromatography mass spectrometer (GC/MS: quadrupole mass spectrometer, SUN200, FAM, attached with a GC, 6890, Agilent) connected to the gas extraction line. The detection limit of the CO_2 and H_2O pressures by the crystal gauge is 0.1 Pa, which, in our analytical setup, corresponds to 8 ppm of C and 1.3 ppm of H.

3.3. Mass Spectrometric Analyses of Carbon Isotopes

[20] A total of 100 mg of rock was reduced to 10–20 μm grain-sized powders with an agate mortar and loaded in a quartz tube with copper oxide. The quartz tube was then sealed under vacuum and the sample combusted at 850°C for 30 min. The produced gas phase was then analyzed for the $^{13}C/^{12}C$ ratio using a stable isotope mass spectrometer SIRA 19 of GV Instruments® at the Université Paris SUD. Analogous to N, the C-isotope ratios are reported as ‰ deviation relative to the Pee Dee Belemnite (PDB) international standard. Total uncertainties on the measurement are of ±0.1‰.

3.4. MC-ICP-MS Techniques for Fe Isotopes Determinations

[21] The Fe isotopic composition of the microbanded iron layers of chert A458 was determined with the goal to understand the origin of these precipitates and its relation with incorporated N and C. All the digestion procedure was done in a class 1000 clean laboratory at GEOTOP, using sub-

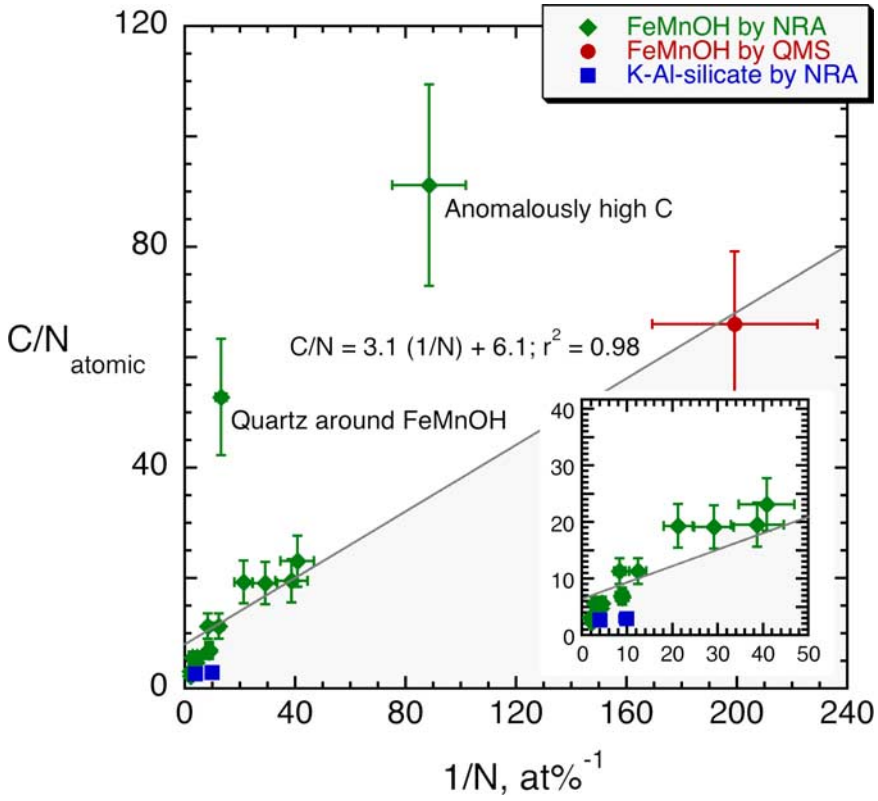

Figure 3. The C/N atomic ratio versus the inverse of the N concentration (expressed as at%) measured in iron oxides and K-Al-silicates by NRA. The red point is the bulk C/N atomic ratio versus the inverse of the N concentration measured in FeMnOH by mass spectrometry. We can see that except sample S8-458Qz and S8-458-Fe, all the NRA data can be explained by the mixing between N and C from FeMnOH and a N-rich component, measured by NRA, which decreases both the original C/N and the 1/N ratio.

boiled acids and Teflon beakers. After a bulk digestion in a mixture of 3 mL concentrated HNO_3 – 1 mL concentrated HF overnight on a hot plate, the sample was evaporated to dryness and then dissolved in a 3 mL concentrated HNO_3-0.2 mL concentrated $HClO_4$ mixture and warm during 24h on a hot plate. After evaporation, the sample is diluted in a 3 mL of concentrated HCl – 0.2 mL of concentrated $HClO_4$, warmed again during 24h and evaporated to dryness. Iron was isolated from the matrix using AGMP-1 anion exchange resin in HCl media, following the procedure described by *Dauphas et al.* [2004].

[22] Iron isotopes were measured using the Multi-collector-ICP-MS Micromass® Isoprobe at the GEOTOP-UQÀM-McGill Research Center. Mass bias corrections were performed using the standard-sample-standard (bracketing) technique with the IRMM014 international isotopic standard as reference. The long-term reproducibility obtained with this technique is on the order of 0.05‰ per atomic mass unit (2σ) and the blank (<50 ng/g) was always negligible compared to the total amount of Fe in the sample. Precision and accuracy were verified by repeat analyses of three reference materials: basalt (BCR 1), granite (AC-E) and BIF from Isua (IF-G). The Fe isotopic composition is expressed in the conventional delta notation ($\delta^{56}Fe \equiv \{[(^{56}Fe/^{54}Fe)_{sample}/(^{56}Fe/^{54}Fe)_{IRMM014}] - 1\} \cdot 1000$)), where the $(^{56}Fe/^{54}Fe)_{IRMM014}$ is equal to 15.69858. The $\delta^{56}Fe$ values measured for the reference materials were +0.63 ± 0.09‰ (2σ, N = 3) for IF-G; +0.33 ± 0.20‰ (2σ, N = 2) for AC-E; and +0.14 ± 0.05‰ (2σ, N = 2) for BCR 1, respectively. Those values are very similar to those previously published [*Beard et al.*, 2003; *Butler et al.*, 2005; *Dauphas and Rouxel*, 2006; *Poitrasson et al.*, 2004; *Rouxel et al.*, 2005].

4. Results

[23] To detect the nitrogen- and carbon-hosting mineral phases, NRA was performed on the following:

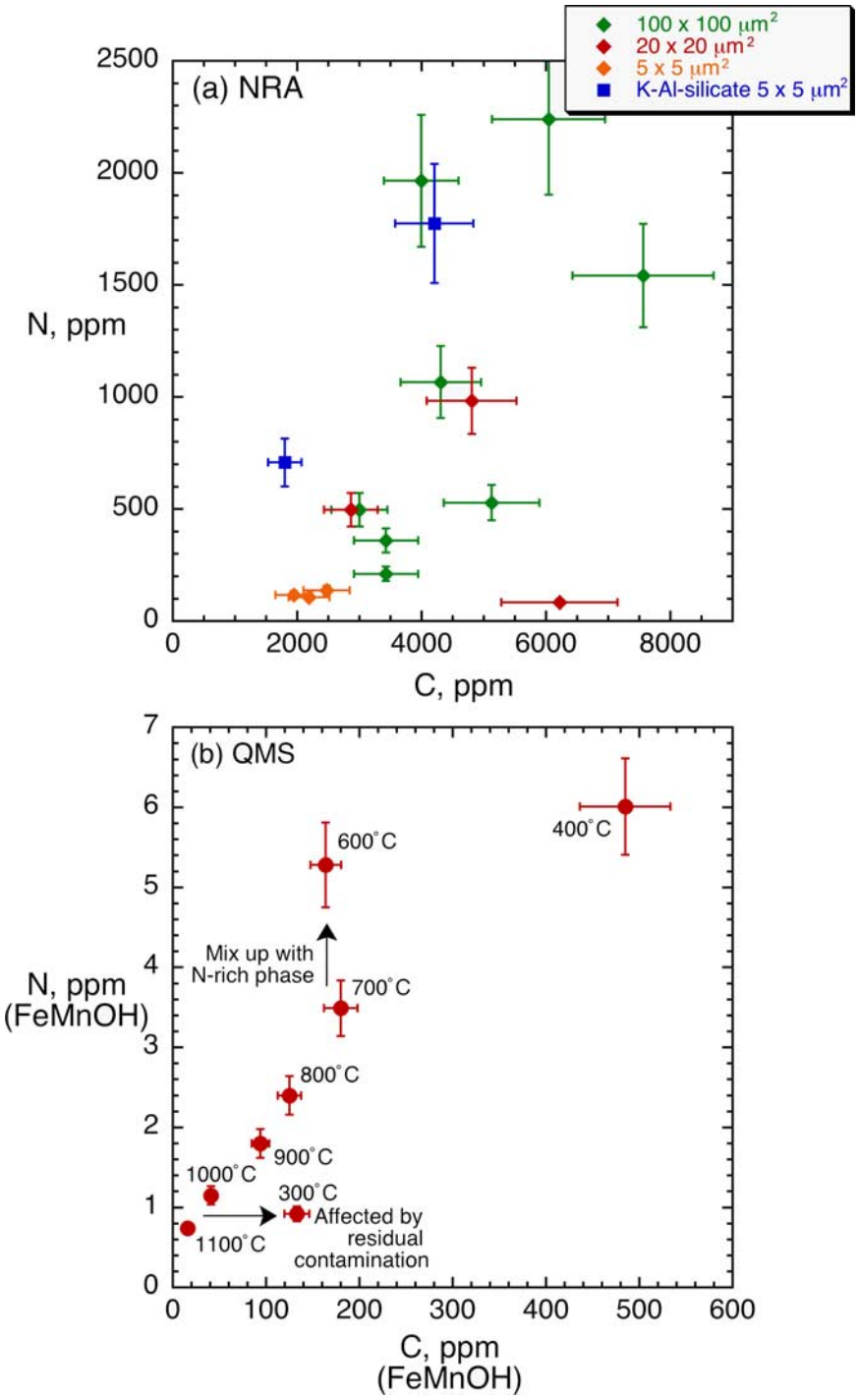

Figure 4. N versus C concentration measured both by NRA (expressed as ppm equivalent) and by mass spectrometry (QMS; expressed as ppm of FeMnOH). Data from NRA measurements for analyses S8-458-Fe are not reported here because of the anomalously large amount of C. While the NRA data do not show a relation between N and C, this relation is significant using QMS data (see text for details about the 300 and 600°C combustion steps).

Table 2. C, N, and Ar Elemental and Isotopic Analyses by QMS of FeMnOH in Chert A458[a]

Temp. Comb., °C	H_2O, ppm	C, ppm	N, ppm	C/N, atomic	$\delta^{15}N$, ‰	±	$^{40}Ar^*$, $\times10^{-8}$ ccSTP/g	±	$^{40}Ar/^{36}Ar$	±
300	867	133	0.92	169	10.5	1.6	1.1	2.6	318	49
400	1524	485	6.01	94	7.1	1.1	12.8	5.5	494	84
500	164	180	3.49	60	9.7	1.13	18.2	6.2	693	134
600	152	164	5.28	36	7.3	0.9	74.1	16.9	1058	173
700	21	125	2.40	61	3.1	0.8	165.3	30.1	3705	622
800	b.l.[a]	94	1.80	61	4.4	1.0	86.1	12.8	2153	277
900	b.l.	41	1.15	42	10.1	1.1	21.1	4.6	1344	246
1000	b.l.	16	0.74	25	10.2	1.1	17.1	3.3	825	161
1100	b.l.	b.l.	0.16	-	13.0	1.8	3.5	1.6	353	31
1200	b.l.	b.l.	0.08	-	20.3	7.4	5.5	2.5	339	34
1200	b.l.	b.l.	0.01	-	b.l.	b.l.	0.1	1.8	303	84
Total	2729	1237	22.02				404.9			

[a] FeMnOH separates weight is 5.86 mg. b.l., blank level.

[24] 1. FeMnOH from the iron bands (Figures 2a and 2b) of zone II and in the crosscutting veins.

[25] 2. Quartz veins and microcrystalline quartz of zone III; quartz filling of zone IV.

[26] 3. Dispersed K-Al-silicates (likely K-feldspars or mica) from the microcrystalline quartz matrix of zone III (Figure 2c).

[27] 4. Fe-sulfides from the chert precipitate (zone III).

[28] N and C were predominantly found in FeMnOH (zone II) and in K-Al-silicates. Microcrystalline quartz does not contain detectable amounts of N. However, the C content in quartz could be estimated to be 0.04 at%, between 2 and 12% of the C content in iron oxides (Table 1). A total of four 100 × 100 μm^2 NRA scans, three 20 × 20 μm^2 microscans and five 5 × 5 μm^2 spots showed detectable amounts of C and N (Table 1, reported as atom (at)% and equivalent ppm).

[29] The amount of N and C measured in FeMnOH ranged between 0.025 to 0.51 at% and between 0.30 to 1.59 at%, respectively (Table 1), but one scan on quartz (sample S8-458-Qz) shows anomalously high carbon concentration of 4.0 at% (1.5 wt% equivalent; Table 1). It is noteworthy that the bulk NRA-based N and C concentrations determined by large-scan analyses are significantly higher than those resulting from small-scan or spot measurements. In particular, nitrogen shows a substantial decrease in concentration from an average of 0.24 at% in larger scans of 100 × 100 μm^2 to 0.11 at% in 20 × 20 μm^2 scans to solely 0.03 at% in 5 × 5 μm^2 spots. Carbon decreases only from 1.2 at% in 100 × 100 μm^2 scans to 0.58 at% in 5 x 5 μm^2 spots (Table 1).

[30] The C/N atomic ratio varies by more than one order of magnitude from 2.3 to 91 (Table 1), with the S8-458 sample having the highest C/N ratio. The two K-rich silicates contain twice as much C and N as the iron oxides but with constant C/N atomic ratios of 2.7 to 2.8 (Table 1). Variations in the C/N ratios are largely due to variations in N contents (Figure 3), and no clear correlation exists between the amounts of C and N measured by NRA (Figure 4a). However, a significant co-variation exists between the concentrations of C and N from FeMnOH as measured by mass spectrometry (Table 2; Figure 4b; except for the step at 300 and 600°C). The C and particularly the N concentrations measured by mass spectrometry, however, differ significantly from those measured by NRA. The total amount of C extracted from FeMnOH is 1237 ppm (0.33 at% equivalent), and it is thus only half of that measured by NRA. Mass spectrometrically determined N amounts of 22 ppm (0.005 at% equivalent) (Table 2) are more than one order of magnitude lower than estimates for the same sample based on NRA (Table 1). This discrepancy will be discussed later.

[31] In Figure 5, we reported concentrations of C, H_2O, N and radiogenic $^{40}Ar^*$, as well as the $\delta^{15}N$ values from FeMnOH as measured by mass spectrometry. Nitrogen is released at 400°C, together with C and H_2O and again at 600°C (Figure 5). The $^{40}Ar^*$ is released mostly at 700°C. $\delta^{15}N$ values were observed at the 400°C and 600°C step not significantly different, with +7.1 ± 1.1‰ and +7.3 ± 0.9‰ respectively. At temperatures higher than 600°C, N release from the sample constantly declines, concomitant with an increase in the $\delta^{15}N$ values from +3.1‰ at 700°C to +20‰ at 1200°C. The combustion pattern of N for the chert

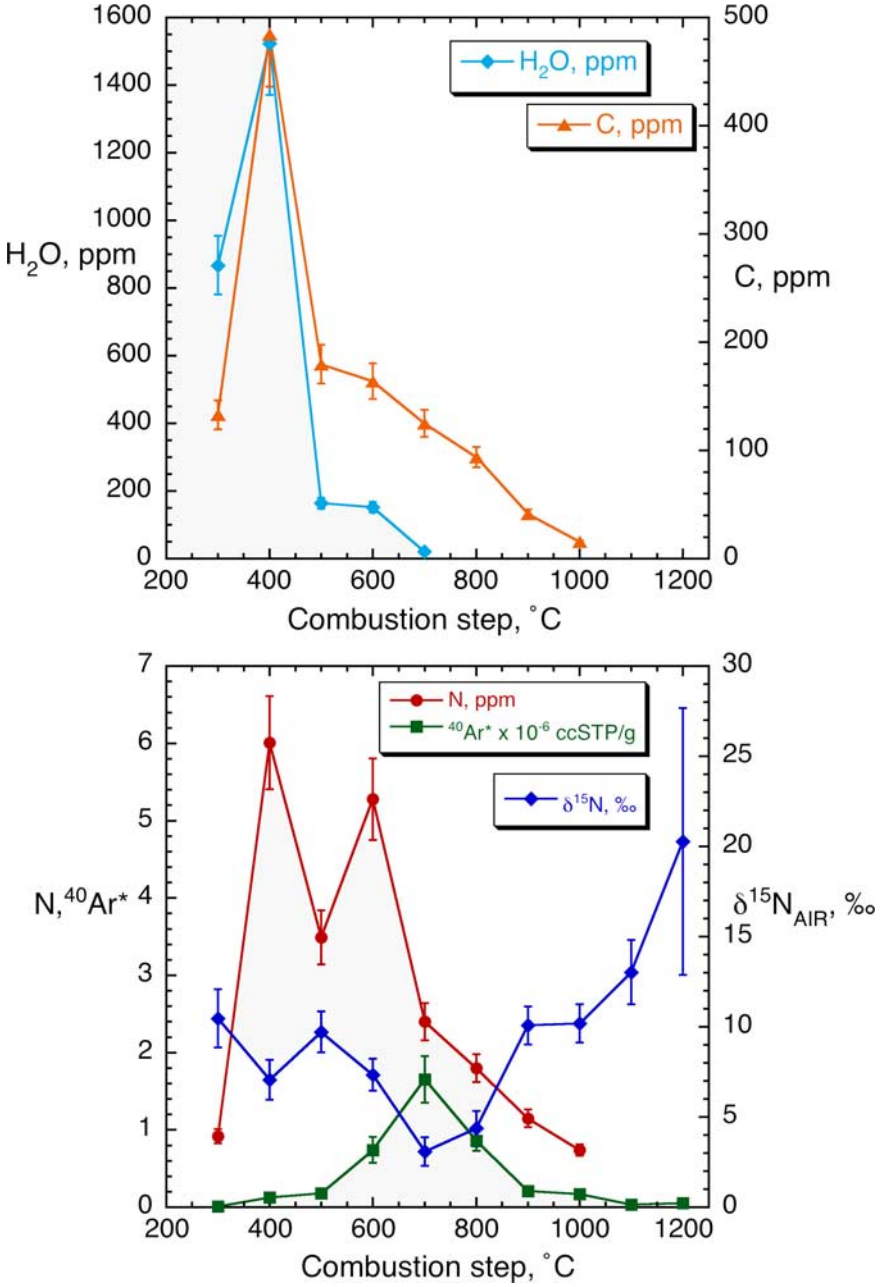

Figure 5. Combustion release pattern for elemental C, H_2O, N, and $^{40}Ar^*$ concentrations reported together with the nitrogen isotopic composition (expressed with the $\delta^{15}N$ notation) for the FeMnOH separates.

A458, between 700°C and 1200°C, is characteristic of a diffusion-controlled fractionation [*Boyd et al.*, 1993]. When N_2 is released from the sample reservoir, the degree of ^{15}N-enrichment is proportional to the log of the fraction f of N_2 remaining in the reservoir. The fraction f can be calculated from the total amount of N released during incremental combustion. Figure 6 depicts the change in $\delta^{15}N$ as a function of the log(f). The $\delta^{15}N$ value correlates well with the yield of N (Figure 6) and the reaction/diffusion rate ratio, k(15)/k(14), for the respective species (molecules or atoms), or fractionation factor can be estimated from: $\delta^{15}N \equiv 1000 \times [k(15)/k(14) - 1] \times \ln(N/N_{initial})$. The slope of the trend in the data yield apparent estimates of k(15)/k(14) of 0.997, indicating a slightly faster release of ^{14}N (3%). The N released between 700°C and 1200°C, had an average $\delta^{15}N$ value of +6.0 ± 0.5‰, slightly lower than the $\delta^{15}N$ value of N released at 400°C (+7.1 ± 1.1‰) and at 600°C (+7.3 ± 0.9‰).

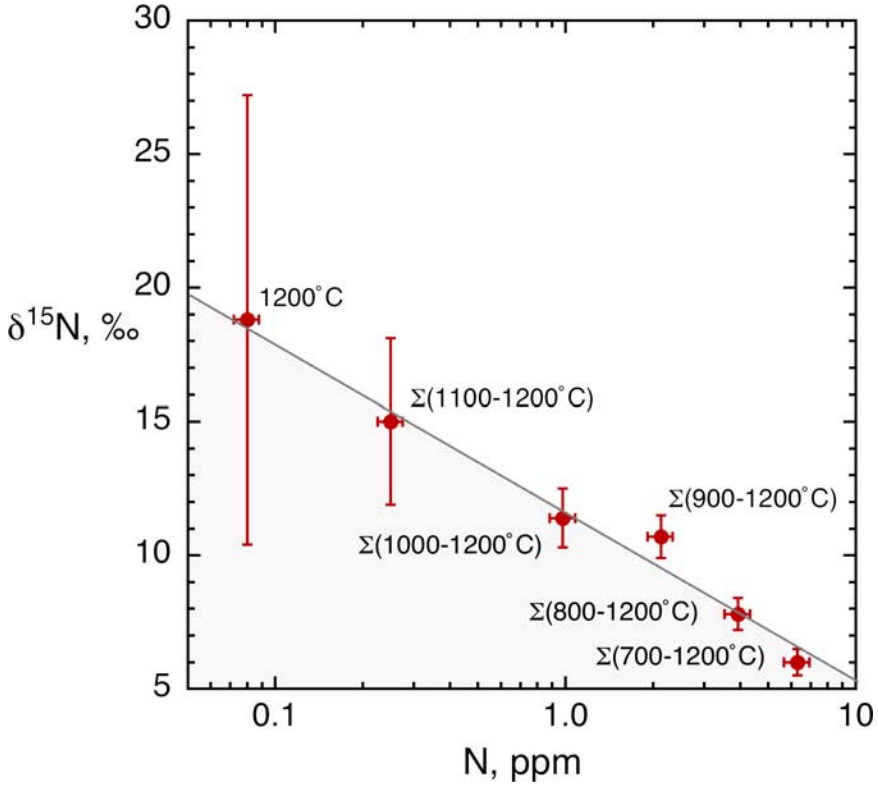

Figure 6. The δ^{15}N values calculated for the sums of remaining steps from 700°C–1200°C to 1100°C–1200°C against the log of the fraction of N remaining in the reservoir. The relation confirms that a Rayleigh distillation process produces the isotopic fractionation of N at high temperatures.

However, given the relatively large errors, the difference cannot be considered significant. The bulk δ^{13}C value measured in the FeMnOH is −19.9 ± 0.1‰.

[32] The ^{40}Ar* and N are not correlated suggesting that radiogenic ^{40}Ar* trapping sites differ from those of N. Finally, Figure 7 shows the Arrhenius plots (the log of the element's amount extracted at each combustion temperature versus the inverse of the extraction temperature) for N and C. Except for the data corresponding to the N released at 1000°C, all data points follow a linear trend, and the slope of the correlation line yield estimates on the activation energy (E_a) of the rate-determining process. For nitrogen, E_a is equal to 18.7 ± 3.7 kJ/mol, which does not differ significantly from the E_a calculated for carbon (13.0 ± 3.8 kJ/mol).

5. Discussion

5.1. Localization of N and C at the Mineral Scale

[33] The large discrepancies with regards to N and C content determined by NRA versus mass spectrometry can most likely be explained in terms of the various intra and inter-crystalline N reservoirs being differently targeted by the two methods. In minerals, volatile elements can (1) be dissolved within grains; (2) be adsorbed on grain boundaries or cleavages; or (3) occur as a separate phase in host minerals, in dislocations or inclusions [*Robert and Halbout*, 1990]. The N and C extracted and analyzed by mass spectrometry are likely bound or dissolved within the crystal structure of the FeMnOH and originate most likely from a common source (see next paragraph). However, the N and C measured by NRA represent a mix between two components. This is clearly illustrated in Figure 3, where the bulk N (calculated as at% equiv.) and the C/N ratio determined by mass spectrometry is plotted together with NRA data. The first end-member component is likely the one bound to, or dissolved in, the FeMnOH. The second end-member is N-rich and its addition has the effect to decrease both the 1/N and the C/N ratio (Figure 3). From the mixing line in Figure 3, the C/N ratio of the N-rich end-member is suggested to be about 6, which is consistent with addition of modern organic contamination (C/N values from 3 to 30) adsorbed

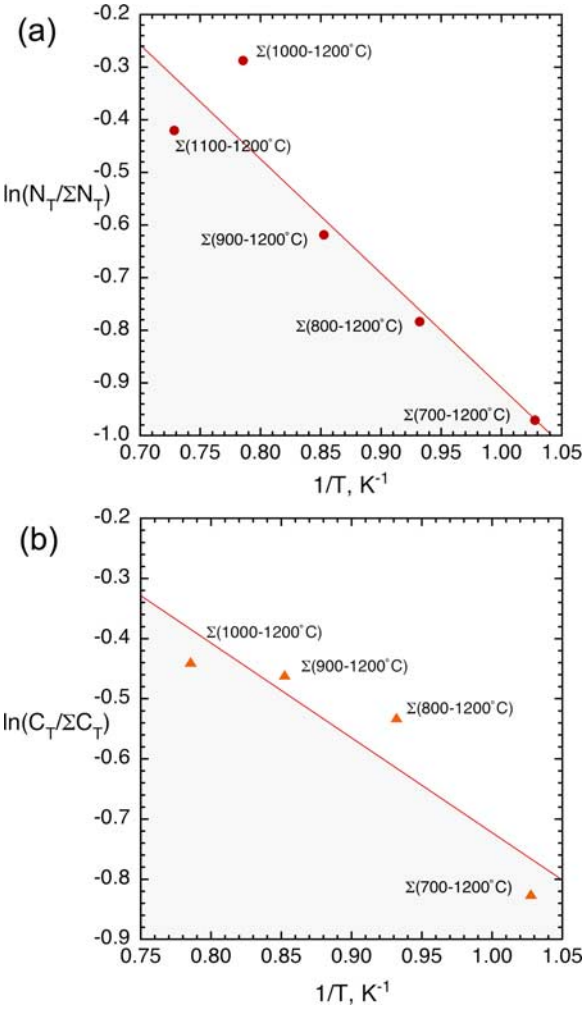

Figure 7. Arrhenius plot of (a) N and (b) C for the FeMnOH separates, confirming that these two elements are released from iron oxides by a diffusion-like process.

on grain surfaces or due to microscopic distinct phases dispersed within these grains. At first sight, an adsorbed component does not seem plausible, given that during NRA, the first micron-size layer is discarded to avoid measuring recent organic contamination. However, combustion experiments in Archean cherts showed that this component deeply permeates the samples and is totally removed only at 400–450°C [*Pinti et al.*, 2001, 2003]. The adsorbed N component accounts for the 18 to 32% of the total N released amount in iron separates [*Pinti et al.*, 2001]. In some case up to 72% of the total released N in Archean metasediments derives from this recent adsorbed component (D. L. Pinti et al., manuscript in preparation, 2007). Thus, while the adsorbed component would not be detected by mass spectrometry (1) because a strict mineral separation was done before analyses and (2) because of overnight pre-combustion of the sample at low temperature that eliminates mostly any adsorbed component, NRA-based N and C determination would include the contribution from contaminant N and C adsorbed below 1μm underneath the surface layer. The fact that two different sources of N and C are targeted by the NRA analyses can explain the inconsistent relation between N and C (Figure 4a). The relation between N and C is rather good during the stepwise combustion because these two species are extracted from a single source (Figure 4b).

5.2. C and N Origin in Iron Layers

[34] The diffusive release of N and C only at relatively high combustion temperatures (Figures 5 and 6) indicates that these elements are firmly embedded in the Fe-oxides, and shielded from the oxygen, which can act to facilitate the release of volatile species. This suggests that N and C were incorporated during the FeMnOH formation, potentially yielding environmental information.

[35] The relatively constant C/N ratio measured by stepwise combustion (Figure 4b) suggests a common organic source of these elements. In Figure 4b, the 300°C and 600°C step data have different C/N ratios. At 300°C, released gases may be contaminated by superficial components, relatively rich in C (as observed by *Pinti et al.* [2001] in other samples), while at 600°C, C/N ratios are probably affected by a second, more N-enriched, organic phase, that admixed to the primary N and C-rich organic phase. It is possible that this second source of organic N is enclosed in quartz, as has been observed in some other cherts [*Pinti et al.*, 2001]. At the temperature of phase transition between α–quartz and β–quartz (573°C), this quartz-bound organic phase would instantaneously be released [*Sano and Pillinger*, 1990].

[36] The measured C/N ratios, the δ^{15}N and δ^{13}C values, all point out to an organic source for N and C. The C/N ratios measured by mass spectrometry range from 53 (integrated value of $C/N_{700-1200°C}$) to 94 (at 400°C step), within the values measured in Archean and Proterozoic kerogens (Figure 8). The corresponding δ^{15}N values ($\delta^{15}N_{700-1200°C} = +6.0 \pm 0.5‰$; $\delta^{15}N_{400°C} = +7.1 \pm 1.1‰$) are at the high end for the Eo-Paleoarchean (Figure 9). *Beaumont and Robert* [1999] showed that ^{15}N-depleted organic matter dominates this period with δ^{15}N values between −6‰ to around 0‰. Compilation of all published data since then by *Shen et al.* [2006]

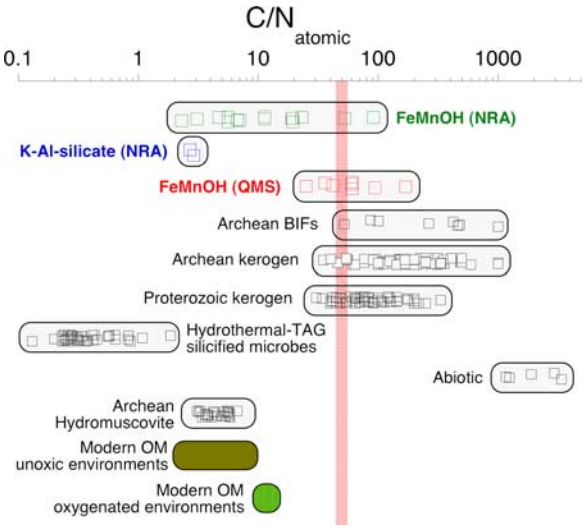

Figure 8. The C/N atomic ratios measured by NRA and QMS in chert A458 (FeMnOH and K-Al-silicates) compared to C/N ratios from literature. Data from Archean and Proterozoic kerogen [*Hayes et al.*, 1983; *Beaumont and Robert*, 1999; *Pinti et al.*, 2001; *Ueno et al.*, 2004; *Jia and Kerrich*, 2004; *van Zuilen et al.*, 2005; *Kerrich et al.*, 2006]; Archean BIF [*Beaumont and Robert*, 1999; *Pinti et al.*, 2001; *Nishizawa et al.*, 2005]; Archean mica from the Panorama Fm. 3460-Myr-old Kitty's Gap chert [*Rouchon et al.*, 2005]; silicified microbes at North Atlantic TAG-4 drill core [*Al-Hanbali et al.*, 2001]; and modern marine organic matter (compilation of literature data from *Shen et al.* [2006]). Data for abiotic formation of C and N are from *van Zuilen et al.* [2006]. The red-stripped area represents the value of C/N for FeMnOH, calculated from the C versus N relation of Figure 4b.

showed that two distinct populations characterize Eo-Paleoarchean with δ^{15}N values centered at −3.6‰ and +4.3‰, respectively. The measured δ^{15}N values in chert A458 are, however, more common during Neoarchean (3.2 to 2.5 Ga; $\delta^{15}N_{mean}$ = +10.8‰ [*Shen et al.*, 2006]), Proterozoic (2.5 to 0.6 Ga; $\delta^{15}N_{mean}$ = +5.6‰; *Shen et al.*, 2006) (Figure 9) or modern times (δ^{15}N = +8.0 ± 2.7‰ [*Shen et al.*, 2006]).

[37] The δ^{13}C value measured in the iron bands of −19.9 ± 0.1‰ suggests also an organic origin. Organic matter in recent marine sediments shows a δ^{13}C value around −20‰ [*Peters et al.*, 1978], compatible with the value found in chert A458, while Archean kerogens show δ^{13}C values centered on −30‰ [*Beaumont and Robert*, 1999]. Several authors [e.g., *Lindsay et al.*, 2005; *van Zuilen et al.*, 2003] have claimed that abiotic processes could produce C with an isotopic signature close to values typical for biologically produced carbon. For example, high-molecular weight organics and kerogen could be abiotically produced by Fischer-Tropsch type reactions during hydrothermal serpentinization of the surrounding basalts. However, recent experiments carried out by *McCollom and Seewald* [2006] showed that the produced organics have a δ^{13}C value much lower (−50‰) than those observed in this study. However, if the carbonaceous matter formed non-biogenically during greenschist facies metamorphism (~300°C), and in isotopic equilibrium with the mantle-derived CO_2, then the δ^{13}C value of this material could be as low as −17‰ [*van Zuilen et al.*, 2006], quite close to −19.9 ± 0.1‰, the value found in chert A458. However, the C/N ratios reported by *van Zuilen et al.* [2006] for abiotic organic compounds from 500 to 4000, would clearly be distinguishable from C/N ratios in biogenic organic matter. Furthermore, in chert A458 the C is intrinsically linked to N (Figure 4b). An abiotic production of N as ammonia through the

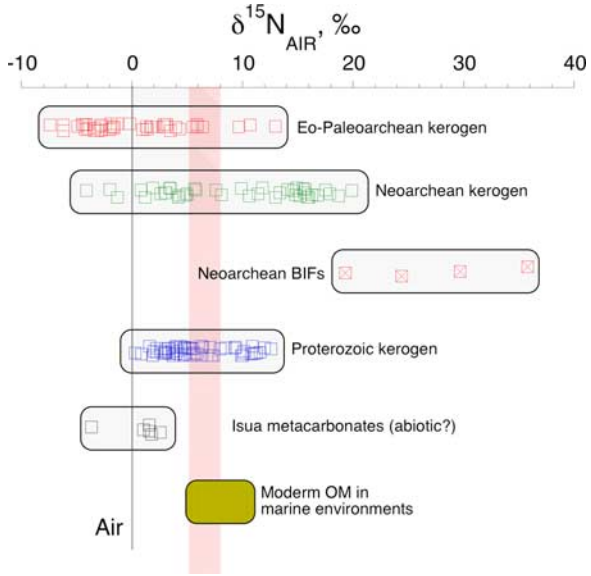

Figure 9. The δ^{15}N values measured by QMS in chert A458 iron layers compared to values measured in Archean and Proterozoic kerogens [*Hayes et al.*, 1983; *Beaumont and Robert*, 1999; *Pinti et al.*, 2001; *Ueno et al.*, 2004; *Jia and Kerrich*, 2004; *van Zuilen et al.*, 2005; *Kerrich et al.*, 2006]; Neoarchean BIFs [*Beaumont and Robert*, 1999; *Pinti et al.*, 2001]; in metacarbonates of Isua, West Greenland [*van Zuilen et al.*, 2005] which could represent abiotic N; and modern marine organic matter [*Shen et al.*, 2006] (compilation of literature data). The dashed line indicates the δ^{15}N value of air; the red-stripped area represents the δ^{15}N value, within uncertainties, of the N component trapped in FeMnOH.

Haber-Bosch process is a very slow reaction and requires high temperatures (400–500°C) and pressures (from 200 bar to several MPa) [*Asperger*, 2003]. There is no indication for such conditions being applicable to the studied samples.

[38] The unusual vermicular internal texture of the FeMnOH (Figure 2d) and the non-stoichiometry of this phase [*Orberger et al.*, 2006b] suggest a microbially mediated crystallization of the iron oxyhydroxides, analogous to some iron formations from modern mid-ocean hydrothermal vents [e.g., *Boyd and Scott*, 2001]. FIB-TEM investigations [*Orberger et al.*, 2006a] showed that the vermicular texture of the FeMnOH is produced by nanofilaments composed of aligned hematite nanoclusters, commonly observed in biologically mediated precipitation of hematite [*Orberger et al.*, 2006a, 2006b]. Within these filaments, carbon nodules of a few nanometers wide have been observed. Electron Energy Loss Spectroscopy (EELS) analyses showed that these C-rich nodules contain also traces of nitrogen [*Orberger et al.*, 2006a]. Further investigations have to be carried out to explain the nature and the origin of these nodules and to confirm that these nodules are the ultimate host of the measured N and C.

[39] So, how is the N (and C) bound in iron oxides? Nitrogen can be adsorbed within the porous structure of Fe-MnOH. The activation energy for the chemisorption of N and C on iron oxides is generally between 20 and 80 kJ/mol [*Burakowski and Wierzchon*, 1998], which is consistent with our observations (see Results). The stepwise-heating release temperature of noble gases trapped in a synthetically grown magnetite is known to be fairly high (~1300°C) [*Matsumoto et al.*, 1996], and the equally high release temperatures for N and C may point to analogous trapping mechanisms for both rare gases as well as N and C. On the basis of model results, *Matsumoto et al.* [1996] proposed that gases are adsorbed at the surface of magnetite grains during the crystal growth, before they are ultimately encapsulated and firmly trapped in the magnetite grain. On the basis of their model, we assume that the component extracted at 400°C (Figure 5) is likely the one adsorbed superficially, while extraction at up to 1200°C and the related diffusion-controlled isotopic fractionation indicate that part of N and C is deeply embedded in the iron oxides.

[40] K-Al-silicates from zone III show C/N ratios of 2.7–2.9, characteristic of those measured in K-Al-silicates from Archean cherts [*Rouchon et al.*, 2005]. The N isotopic composition in these silicates was not analyzed because of the separation difficulties related to its fine intergrowth with microcrystalline quartz matrix of zone III (Figure 2c). However, *Pinti et al.* [2001] measured the N isotopic composition of the A458 on a selected aliquot of pure quartz, which may be representative for zone III. A nitrogen release peak at 1200°C was observed, associated with a release of radiogenic $^{40}Ar^*$ which could indicate the occurrence of NH_4^+ bounded in K-feldspars [*Boyd et al.*, 1993]. This component has a $\delta^{15}N$ value of +12.1 ± 2.9‰, but it is still unclear whether its isotopic value has been affected by post-depositional devolatilization [*Pinti et al.*, 2001].

5.3. Organic Nitrogen and Carbon: Pristine or Later Addition?

[41] If the N and C in the Marble Bar chert is originally derived from the degradation of organic matter, the question arises when and how they were incorporated into the chert. This study shows that both N and C are part of the mineral structure of the iron oxides, implying their incorporation at the time of the FeMnOH precipitation.

[42] The iron isotopic composition of the two microbanded iron layers ($\delta^{56}Fe = -0.38 \pm 0.02$‰) is similar to that measured in hot (>300°C) hydrothermal fluids from mid-ocean ridges ($\delta^{56}Fe = -0.5$ to -0.2‰) [e.g., *Sharma et al.*, 2001; *Severmann et al.*, 2004]. The hydrothermal origin of the these iron oxide-rich microbands in chert A458 is also confirmed by the enrichment in Mn and most of the REE and the occurrence of pronounced Eu anomalies [*Orberger et al.*, 2006b].

[43] These low-temperature FeMnOH deposits can form at the mid-ocean ridges through two different mechanisms: (1) the reaction of basalts in the upper oceanic crust with oxygenated deep-seawater and the subsequent low-temperature formation of secondary minerals including Fe oxyhydroxides, smectite, and celadonite [*Alt*, 1995] and (2) the direct precipitation of iron oxides from the hydrothermal plume when it enters oxygenated waters. Present-day examples of the first case are composed mainly of silica (quartz), and Fe-oxyhydroxides showing variable $\delta^{56}Fe$ values between −1.6 and +0.3‰ [*Rouxel et al.*, 2003]. These variations have been interpreted to result from the effects of Rayleigh distillation kinetics on the Fe-isotope fractionation during Fe-oxyhydroxide precipitation and/or during partial oxidation of hydrothermal

Fe^{2+}. In contrast, Fe-oxyhydroxide-rich sediments precipitated directly from the hydrothermal plume (case 2 above) display δ^{56}Fe values that are indistinguishable from the δ^{56}Fe values found for high-temperature hydrothermal fluids (−0.5 to −0.2‰), indicating that the original isotopic composition of the vent fluid is preserved when $Fe(II)_{aq}$ oxidation in seawater is complete [*Dauphas and Rouxel*, 2006].

[44] Our δ^{56}Fe data are consistent with both scenarios, yet we prefer on the basis of the close similarity of the δ^{56}Fe values found from this study and those of hot hydrothermal fluids as well as other characteristics that the FeMnOH precipitated directly from a hydrothermal plume. Supporting evidence comes from the Th/U ratio of the Marble Bar chert which is close to unity. *Cloquet et al.* [2006] showed that BIFs produced by direct precipitation from a hydrothermal effluent have Th/U ratios ranging from 0.2 to 1.2, thus consistent with our value. Residual iron oxides derived from weathering show higher Th/U ratios (up to 10) due to the higher mobility of U rather than Th, during alteration processes [*Cloquet et al.*, 2006]. Finally, the N isotopic composition of FeMnOH from Marble Bar chert does not match with those expected from basalt weathering. Indeed, *Busigny et al.* [2005] showed that Fe-oxyhydroxide facies in altered basalt from modern oceanic crust contain NH_4^+ located in secondary minerals such as K-bearing celadonite and smectite and showing δ^{15}N values ranging from −3.8‰ to −2.7‰. The decoupling between radiogenic ^{40}Ar* and N indicates clearly that K-bearing minerals are not the principal host of N in the Marble Bar chert. All these evidences support a direct precipitation of FeMnOH from a hot hydrothermal effluent at Marble Bar, rather than the product of ancient or modern basalt weathering.

[45] The determination of the absolute age of FeMnOH formation has obviously important implications for the age of the organic matter and its biogenic traces. On the basis of earlier work of *Barley* [1993], the silicification of the sedimentary sequences of the Warrawoona group in Pilbara Craton by pervasive hydrothermal fluids is produced within 300 Myr from the age of their formation. Because the iron isotope composition of the FeMnOH seems to exclude the secondary origin by recent weathering, we consider that these iron oxides precipitated during the main hydrothermal pulses which produced the Marble Bar cherty units. The Marble Bar's FeMnOH could theoretically be dated by the K-Ar method, since traces of K (0.01 to 0.09 wt% [*Orberger et al.*, 2006b]), and radiogenically produced ^{40}Ar* (Table 2) are found. However, we consider that N in FeMnOH most likely predates the formation of Ar-bearing phases because of the following: (1) The K concentration in Fe is heterogeneous. Laser ablation ICP-MS analyses on two iron microbands located in the lower part of the sample (Figure 2a) found that K in the Fe-microbands varied significantly, ranging from 63 ± 37 ppm to 1420 ± 621 ppm. (2) The absence of relationship between N and ^{40}Ar* indicates the decoupling of these two elements.

[46] This study is limited to one sample, yet the occurrence of a primitive organic N with a positive δ^{15}N value in chert A458 has important implications on the continuing debate on the evolution of the nitrogen biogeochemical cycle and its relation with past changes of the redox state of the primitive oceans and atmosphere [*Shen et al.*, 2006, and references therein]. As mentioned above, Eo-Paleoarchean organic matter is characterized by N with δ^{15}N values between −7‰ to 0‰ [*Beaumont and Robert*, 1999; *Pinti et al.*, 2001, 2003; *Ueno et al.*, 2004; *Papineau et al.*, 2005; *Hashizume et al.*, 2006]. This nitrogen could derive from the mantle, and metabolized by chemosynthetic communities living close to hydrothermal systems, in fully agreement with the depositional environments of the N-host rocks [*Pinti and Hashizume*, 2001]. A ^{15}N-enriched composition like in chert A458 is usually found in later periods, from Neoarchean to Proterozoic, and beyond, when the oceans were progressively oxygenated and the biological production of oceanic nitrates (NO_3^-) with characteristic δ^{15}N values around +7‰ was enhanced [*Peters et al.*, 1978].

[47] Positive δ^{15}N values in earlier Archean times are difficult to explain. One explanation could be that the nitrogen isotopic composition of the pristine organic matter was sensibly ^{15}N-depleted (δ^{15}N values of ≈−6‰) and then it has been fractionated toward higher values during incorporation in iron oxides. *Shen et al.* [2006] have indeed noticed that the N isotopic composition in banded iron formations is extremely high, from +20‰ to +35‰. This has been confirmed by recent work on a Neoarchean BIFs from the Dharwar craton, India by *Cloquet et al.* [2006] that showed δ^{15}N values as high as +22‰. However, the cause of this fractionation is still unclear [*Shen et al.*, 2006]. The alternative hypothesis is that the N isotopic composition reflects biological fraction-

ation similar to that produced in the modern oxygenated ocean by the assimilation-nitrification-denitrification cycle. Recent geochemical studies on Marble Bar unaltered samples recovered from the Archean Biosphere Drilling Project (ABDP) borehole suggest that the iron oxides within Marble Bar cherts are derived from reactions with oxygenated waters [*Ohmoto et al.*, 2004]. These environmental conditions, although localized, could have enhanced the presence of nitrifiers. It is clear that such a hypothesis would have dramatic consequences on the ongoing debate of the oxygenation of the Earth [e.g., *Holland*, 2002], and further investigations are needed to univocally determine the age of the N (and C) incorporation in Marble Bar cherts.

6. Conclusions

[48] In this contribution, we identified the mineralogical sites where bioindicative elements, such as N and C, reside within a rock. We have done this by using a combination of new developed in situ analytical methods for detecting N and C at mineral scale and routine measurements of their isotopic composition using the stepwise combustion method. Such a work is the first step toward a correct interpretation of the N and C sources and fate during rock diagenesis, weathering and metamorphism and of their isotopic composition in term of biogenicity.

[49] Analyses on separate mineral phases from a well-studied Archean chert of Marble Bar, Western Australia confirmed that N and C is tightly retained within iron oxides. This is an important finding, because biogenic N and C, encapsulated within iron oxide mineral sites, could be better protected from post-depositional weathering and metamorphic events. This may help in preserving their pristine isotopic composition, yielding important environmental information. This study showed that the N and C isotopic composition ($\delta^{15}N \approx +6‰$ and $\delta^{13}C \approx -20‰$) and the C/N elemental ratio (C/N = 52) in FeMnOH of the Marble Bar chert are similar to that of organic matter preserved in modern marine sediments. The Fe isotopic composition of these oxides also permits to suggest a direct precipitation of Fe-oxides from reactions of Fe-rich hydrothermal plumes with locally oxygenated waters. These reactions likely took places during the earlier hydrothermal pulses affecting the Marble Bar Formation, rather than derived from modern basalt weathering. This has important consequences on the interpretation on the isotopic composition of N and C which point out the possibility to have in early times, oasis of oxygenated waters where biosynthesis of N and C worked in a way similar to modern times.

Acknowledgments

[50] Comments and suggestions from Y. Sano an anonymous reviewer and the handling editor (V. Salters) greatly improved the manuscript. We are deeply indebted to Moritz Lehmann (GEOTOP), who reworked the text and gave thoughtful comments that helped in clarifying several issues. Bill Minarik is thanked for his precious help during laser ablation ICP-MS measurements of potassium at McGill University. Help from Akiyo Sugihara in treatment of the sample prior to the N mass spectrometry is appreciated. L. Delabesse is thanked for the microphotographs, Michelle Laithier is thanked for redrawing figures, and the staff of Pierre Süe Laboratory is thanked for helping during NRA analyses. Funds from the CNRS-INSU-CNES National Program of Planetology, the CNRS-GDR Exobiology, the GEOTOP-UQÀM-McGill supported D.L.P., B.O., and Ch.C. research. Grant-in-Aid for Science Research from MEXT/JSPS (grants 14702016 and 17340168) supported K.H. NSERC Discovery Grant 314496-05 funded D.L.P. to stay at Osaka University in June 2006 to finish this work. This is GEOTOP contribution 2007-002.

References

Al-Hanbali, H. S., S. J. Sowerby, and N. G. Holm (2001), Biogenicity of silicified microbes from a hydrothermal system: Relevance to the search for evidence of life on earth and other planets, *Earth Planet. Sci. Lett.*, *191*, 213–218.

Alt, J. C. (1995), Subseafloor processes in mid-ocean ridge hydrothermal systems, in *Seafloor Hydrothermal Systems: Physical, Chemical, Biological, and Geological Interactions*, *Geophys. Monogr. Ser.*, vol. 91, edited by S. E. Humphris et al., pp. 85–114, AGU, Washington, D. C.

Asperger, S. (2003), *Chemical Kinetics and Inorganic Reaction Mechanisms*, 361 pp., Springer, New York.

Banfield, J. F., and H. Zhang (2001), Nanocrystals as model systems for pressure-induced structural phase transitions, in *Nanoparticles and the Environment, Reviews of Mineralogy and Geochemistry*, vol. 44, edited by J. F. Banfield and A. Navrotsky, pp. 1–51, Mineral. Soc. of Am., Washington, D. C.

Barley, M. E. (1993), Volcanic, sedimentary and tectonostratigraphy environments of the ~3.46 Ga Warrawoona Megasequence: A review, *Precambrian Res.*, *60*, 47–67.

Beard, B. L., C. M. Johnson, J. L. Skulan, K. H. Nealson, L. Cox, and H. Sun (2003), Application of Fe isotopes to tracing the geochemical and biological cycling of Fe, *Chem. Geol.*, *196*, 43–56.

Beaumont, V., and F. Robert (1999), Nitrogen isotope ratios of kerogens in Precambrian cherts: A record of the evolution of atmosphere chemistry?, *Precambrian Res.*, *96*, 63–82.

Boyd, S. R. (2001), Ammonium as a biomarker in Precambrian metasediments, *Precambrian Res.*, *108*, 159–173.

Boyd, S. R., and P. Philippot (1998), Precambrian ammonium biogeochemistry: A study of the Moine metasediments, Scotland, *Chem. Geol.*, *144*, 257–268.

Boyd, S. R., A. Hall, and C. T. Pillinger (1993), The measurement of $\delta^{15}N$ in crustal rocks by static vacuum mass spectrometry–Application to the origin of the ammonium in the Cornubian Batholith, southwest England, *Geochim. Cosmochim. Acta*, *57*, 1339–1347.

Boyd, T. D., and S. D. Scott (2001), Microbial and hydrothermal aspects of ferric oxyhydroxides and ferrosic hydroxides: The example of Franklin Seamount, Western Woodlark Basin, Papua New Guinea, *Geochem. Trans.*, *7*, doi:10.1039/b105277m.

Burakowski, T., and T. Wierzchon (1998), *Surface Engineering of Metals: Principles, Equipment and Technologies*, CRC Press, Boca Raton, Fla.

Busigny, V., P. Cartigny, P. Philippot, M. Ader, and M. Javoy (2003), Massive recycling of nitrogen and other fluid-mobile elements (K, Rb, Cs, H) in a cold slab environment: Evidence from HP to UHP oceanic metasediments of the Schistes Lustres nappe (western Alps, Europe), *Earth Planet. Sci. Lett.*, *215*, 27–42.

Busigny, V., C. Laverne, and M. Bonifacie (2005), Nitrogen content and isotopic composition of oceanic crust at a superfast spreading ridge: A profile in altered basalts from ODP Site 1256, Leg 206, *Geochem. Geophys. Geosyst.*, *6*, Q12O01, doi:10.1029/2005GC001020.

Butler, I. B., C. Archer, D. Vance, A. Oldroyd, and D. Rickard (2005), Fe isotope fractionation on FeS formation in ambient aqueous solution, *Earth Planet. Sci. Lett.*, *236*, 430–442.

Cloquet, C., D. L. Pinti, B. Orberger, K. Hashizume, and V. Rouchon (2006), Iron isotopic composition of iron-silica layers along a profile in a single ~2.9Ga old BIF from Dharwar Craton, Southern India, paper presented at the 2006 Annual Meeting of the Association Geologique du Canada and Association Mineralogique du Canada, Montréal, Canada, 14 –17 May .

Daudin, L., H. Khodja, and J. P. Gallien (2003), Development of "position-charge-time" tagged spectrometry for ion beam microanalysis, *Nucl. Instrum. Methods Phys. Res., Sect. B*, *210*, 153–158.

Dauphas, N., and B. Marty (2004), "A large secular variation in the nitrogen isotopic composition of the atmosphere since the Archaean?" response to a comment on "The nitrogen record of crust-mantle interaction and mantle convection from Archaean to Present" by R. Kerrich and Y. Jia, *Earth Planet. Sci. Lett.*, *225*, 441–450.

Dauphas, N., and O. Rouxel (2006), Mass spectrometry and natural variations of iron isotopes, *Mass Spectrom. Rev.*, *25*, 515–550.

Dauphas, N., P. E. Janney, R. A. Mendybaev, M. Wadhwa, F. M. Richter, A. M. Davis, M. van Zuilen, R. Hines, and C. N. Foley (2004), Chromatographic separation and multicollection-ICPMS analysis of Iron. Investigating mass-dependent and independent isotope effects, *Anal. Chem.*, *76*, 5855–5863.

de Ronde, C. E. J., D. M. D. Channer, K. Faure, C. J. Bray, and T. C. Spooner (1997), Fluid chemistry of Archean seafloor hydrothermal vents: Implications for the composition of circa 3.2 Ga seawater, *Geochim. Cosmochim. Acta*, *61*, 4025–4042.

de Wit, M., R. Hart, A. Martin, and P. Abbott (1982), Archean abiogenic and probable biogenic structures associated with mineralized hydrothermal vent systems and regional metasomatism, with implications for greenstone belt studies, *Econ. Geol.*, *77*, 1783–1802.

Freudenthal, T., T. Wagner, F. Wenzhofer, M. Zabel, and G. Wefer (2001), Early diagenesis of organic matter from sediments of the eastern subtropical Atlantic: Evidence from stable nitrogen and carbon isotopes, *Geochim. Cosmochim. Acta*, *65*, 1795–1808.

Gallien, J. P., B. Orberger, L. Daudin, D. L. Pinti, and J. Pasava (2004), Nitrogen in biogenic and abiogenic minerals from Paleozoic black shales: An NRA study, *Nucl. Instrum. Methods Phys. Res., Sect. B*, *217*, 113–122.

Hashizume, K., and N. Sugiura (1990), Precise measurement of nitrogen isotopic composition using a quadrupole mass spectrometer, *Mass Spectrosc.*, *38*, 269–286.

Hashizume, K., A. Sugihara, D. L. Pinti, B. Orberger, and F. Westall (2006), Search for primordial biogenic isotopic signatures of nitrogen in Archean sedimentary rocks, *Geochim. Cosmochim. Acta*, *70*, suppl. 1, A235.

Hayes, J. M., I. R. Kaplan, and K. W. Wedeking (1983), Precambrian organic geochemistries, preservation of the record, in *Earth's Earliest Biosphere*, edited by W. J. Schopf, pp. 92–134, Cambridge Univ. Press, New York.

Hofmann, A. (2005), The geochemistry of sedimentary rocks from the Figure Tree Group, Barberton greenstone belt: Implications for tectonic, hydrothermal and surface processes during mid-Archaean times, *Precambrian Res.*, *143*, 23–49.

Holland, H. D. (2002), Volcanic gases, black smokers, and the great oxidation event, *Geochim. Cosmochim. Acta*, *66*, 3811–3826.

Honma, H. (1996), High ammonium contents in the 3800 Ma Isua supracrustal rocks, central west Greenland, *Geochim. Cosmochim. Acta*, *60*, 2173–2178.

Honma, H., and Y. Itihara (1981), Distribution of ammonium in minerals of metamorphic and granitic rocks, *Geochim. Cosmochim. Acta*, *45*, 983–988.

Jia, Y., and R. Kerrich (2004), Nitrogen 15-enriched Precambrian kerogen and hydrothermal systems*Geochem. Geophys. Geosyst.*, *5*, Q07005, doi:10.1029/2004GC000716.

Kato, Y., and K. Nakamura (2003), Origin and global tectonic significance of Early Archean cherts from the Marble Bar greenstone belt, Pilbara Craton, Western Australia, *Precambrian Res.*, *125*, 191–243.

Kerrich, R., Y. Jia, C. Manikyamba, and M. Naqvi (2006), Secular variations of N-isotopes in terrestrial reservoirs and ore deposits, in *Evolution of Early Earth's Atmosphere, Hydrosphere, and Biosphere—Constraints from Ore Deposits*, edited by S. E. Kesler, and H. Ohmoto, *Mem. Geol. Soc. Am.*, *198*, 81–104.

Khodja, H., E. Berthoumieux, L. Daudin, and J. P. Gallien (2001), The Pierre Sue Laboratory nuclear microprobe as a multi-disciplinary analysis tool, *Nucl. Instrum. Methods Phys. Res., Sect. B*, *181*, 83–86.

Lehmann, M. F., S. M. Bernasconi, A. Barbieri, and J. A. McKenzie (2002), Preservation of organic matter and alteration of its carbon and nitrogen isotope composition during simulated and in situ early sedimentary diagenesis, *Geochim. Cosmochim. Acta*, *66*, 3573–3584.

Lindsay, J. F., M. D. Brasier, N. McLoughlin, O. R. Green, M. Fogel, A. Steele, and S. A. Mertzman (2005), The problem of deep carbon–An Archean paradox, *Precambrian Res.*, *143*, 1–22.

Matsumoto, T., K. Maruo, A. Tsuchiyama, and J. Matsuda (1996), Occlusion of noble gases (He, Ne, Ar, Kr, Xe) into synthetic magnetite at 500–1300°C, *Earth Planet. Sci. Lett.*, *141*, 315–324.

McCollom, T. M., and J. S. Seewald (2006), Carbon isotope composition of organic compounds produced by abiotic synthesis under hydrothermal conditions, *Earth Planet. Sci. Lett.*, *243*, 74–84.

Mosbah, M., A. Bastoul, M. Cuney, and J. Pironon (1993), Nuclear microprobe analysis of ^{14}N and its application to the

study of ammonium-bearing minerals, *Nucl. Instrum. Methods Phys. Res., Sect. B*, *77*, 450–456.

Nishizawa, M., N. Takahata, K. Terada, T. Komiya, Y. Ueno, and Y. Sano (2005), Lead, carbon and nitrogen isotope geochemistry of apatite-bearing metasediments from 3.8 Ga Isua supracrustal belt, West Greenland: Primary signature and secondary disturbance, *Int. Geol. J.*, *47*, 952–970.

Ohmoto, H., D. C. Bevacqua, Y. Watanabe, and T. Otake (2004), Origins of carbonaceous matter, hematite, and pyrite in the 3.46Ga Marble Bar chert/jasper/basalt Formation, Pilbara, Western Australia, *Eos, Trans. AGU*, *85*(47), Abstract B32B-02.

Orberger, B., J. P. Gallien, D. L. Pinti, M. Fialin, L. Daudin, D. R. Grocke, and J. Pasava (2005), Nitrogen and carbon partitioning in diagenetic and hydrothermal minerals from Paleozoic Black Shales (Selwyn Basin, Yukon Territories, Canada), *Chem. Geol.*, *218*, 249–264.

Orberger, B., et al. (2006a), Biomarkers in Archaean banded iron formations from Pilbara and Dhawar Craton, *Geochim. Cosmochim. Acta*, *70*, suppl. 1, A461.

Orberger, B., V. Rouchon, F. Westall, S. T. de Vries, D. L. Pinti, C. Wagner, R. Wirth, and K. Hashizume (2006b), Microfacies and origin of some Archaean cherts (Pilbara, Australia), in Processes on the Early Earth, edited by W. U. Reimold and L. R. Gibson, *Spec. Pap. Geol. Soc. Am.*, *405*, 133–156.

Orberger, B., A. Vymazalova, C. Wagner, M. Fialin, J. P. Gallien, R. Wirth, G. Montagnac, and J. Pasava (2006c), Origin of MoSC phases in Lower Cambrian black shales (Southern China), *Geochim. Cosmochim. Acta*, *70*, suppl. 1, A462.

Papineau, D., S. J. Mojzsis, J. A. Karhu, and B. Marty (2005), Nitrogen isotopic composition of ammoniated phyllosilicates: Case studies from Precambrian metamorphosed sedimentary rocks, *Chem. Geol.*, *216*, 37–58.

Paris, I., I. G. Stranistreet, and M. J. Huges (1985), Cherts of the Barberton Greenstone Belt interpreted as products of submarine exhalative activity, *J. Geol.*, *93*, 111–130.

Perry, E. C. J., and L. Lefticariu (2003), Formation and geochemistry of Precambrian cherts, in *Sediments, Diagenesis, and Sedimentary Rocks*, *Treatise Geochem.*, vol. 7, edited by F. T. MacKenzie, p. 99–113, Elsevier, New York.

Peters, K. E., R. E. Sweeney, and I. R. Kaplan (1978), Correlation of carbon and nitrogen stable isotope ratios in sedimentary organic matter, *Limnol. Oceanogr.*, *23*, 598–604.

Pinti, D. L., and K. Hashizume (2001), N-15-depleted nitrogen in Early Archean kerogens: Clues on ancient marine chemosynthetic-based ecosystems? A comment to Beaumont,V., Robert, F., 1999. Precambrian Res. 96, 62–82, *Precambrian Res.*, *105*, 85–88.

Pinti, D. L., K. Hashizume, and J. Matsuda (2001), Nitrogen and argon signatures in 3.8 to 2.8 Ga metasediments: Clues on the chemical state of the Archean ocean and the deep biosphere, *Geochim. Cosmochim. Acta*, *65*, 2301–2315.

Pinti, D. L., K. Hashizume, P. Philippot, J. Foriel, and P. Rey (2003), Nitrogen quest in Archean metasediments of Pilbara, Australia, *Geochim. Cosmochim. Acta*, *67*, A379.

Poitrasson, F., A. N. Halliday, D. C. Lee, S. Levasseur, and N. Teutsch (2004), Iron isotope differences between Earth, Moon, Mars and Vesta as possible records of contrasted accretion mechanisms, *Earth Planet. Sci. Lett.*, *223*, 253–266.

Robert, F., and J. Halbout (1990), A numerical model for isotopic patterns from thermal-extraction experiments, *Meteoritics*, *25*, 291–299.

Rouchon, V., B. Orberger, D. L. Pinti, F. Westall, and J. P. Gallien (2004), Kitty's Gap (Pilbara, Australia) silicified pyroclastites: Preservation of early alteration products?, in *Field Forum on Processes on the Early Earth*, edited by W. U. Reimold and A. Hofmann, pp. 80–81, Geol. Soc. of Am, Boulder, Colo.

Rouchon, V., D. L. Pinti, J. P. Gallien, B. Orberger, L. Daudin, and F. Westall (2005), NRA analyses of N and C in hydromuscovite aggregates from a 3.5 Ga chert from Kitty's Gap, Pilbara, Australia, *Nucl. Instrum. Methods Phys. Res., Sect. B*, *231*, 536–540.

Rouxel, O., N. Dobbek, J. Ludden, and Y. Fouquet (2003), Iron isotope fractionation during oceanic crust alteration, *Chem. Geol.*, *202*, 155–182.

Rouxel, O., A. Bekker, and K. Edwards (2005), Iron isotope constraints on the Archean and Paleoproterozoic ocean redox state, *Science*, *307*, 1088–1091.

Sano, Y., and C. T. Pillinger (1990), Nitrogen isotopes and N_2/Ar ratios in cherts: An attempt to measure time evolution of atmospheric δ^{15}N value, *Geochem. J.*, *24*, 315–325.

Severmann, S., C. M. Johnson, B. L. Beard, C. R. German, H. N. Edmonds, H. Chiba, and D. R. H. Green (2004), The effect of plume processes on the Fe isotope composition of hydrothermally derived Fe in the deep ocean as inferred from the Rainbow vent site, Mid-Atlantic Ridge, 36 degrees 14′ N, *Earth Planet. Sci. Lett.*, *225*, 63–76.

Sharma, M., M. Polizzotto, and A. D. Anbar (2001), Iron isotopes in hot springs along the Juan de Fuca Ridge, *Earth Planet. Sci. Lett.*, *194*, 39–51.

Shen, Y., D. L. Pinti, and K. Hashizume (2006), Biogeochemical cycles of sulfur and nitrogen in the Archean ocean and atmosphere, in *Archean Geodynamics and Environments*, *Geophys. Monogr. Ser.*, vol. 164, edited by K. Benn et al., pp. 305–320, AGU, Washington, D. C.

Siever, R. (1992), The silica cycle in the Precambrian, *Geochim. Cosmochim. Acta*, *56*, 3265–3272.

Sugitani, K. (1992), Geochemical characteristics of Archean cherts and other sedimentary rocks in the Pilbara Block, Western Australia: Evidence for Archean seawater enriched in hydrothermally-derived iron and silica, *Precambrian Res.*, *57*, 21–47.

Thorpe, R. I., A. H. Hickman, D. W. Davis, J. K. Mortensen, and A. F. Trendall (1992), U-Pb zircon geochronology of Archean felsic units in the Marble Bar Region, Pilbara Craton, Western-Australia, *Precambrian Res.*, *56*, 169–189.

Ueno, Y., H. Yoshioka, S. Maruyama, and Y. Isozaki (2004), Carbon isotopes and petrography of kerogens in similar to 3.5-Ga hydrothermal silica dikes in the North Pole area, Western Australia, *Geochim. Cosmochim. Acta*, *68*, 573–589.

Van Kranendonk, M. J., A. H. Hickman, I. R. Williams, and W. Nijman (2001), Archaean geology of the East Pilbara granite-greenstone terrane, Western Australia–A field guide, *Record 2001/9*, 134 pp., Geol. Surv. W. Aust., Perth, Australia.

van Zuilen, M. A., A. Lepland, J. Teranes, J. Finarelli, M. Wahlen, and G. Arrhenius (2003), Graphite and carbonates in the 3.8 Ga old Isua Supracrustal Belt, southern West Greenland, *Precambrian Res.*, *126*, 331–348.

van Zuilen, M. A., K. Mathew, B. Wopenka, A. Lepland, K. Marti, and G. Arrhenius (2005), Nitrogen and argon isotopic signatures in graphite from the 3.8-Ga-old Isua Supracrustal Belt, Southern West Greenland, *Geochim. Cosmochim. Acta*, *69*, 1241–1252.

van Zuilen, M. A., M. Chaussidon, C. Rollion-Bard, B. Luais, and B. Marty (2006), Carbonaceous cherts of the Barberton Greenstone Belt, South Africa, *Geophys. Res. Abstr.*, *8*, 04975.

Yamamoto, T., K. Hashizume, J. Matsuda, and T. Kase (1998), Multiple nitrogen isotopic components co-existing in ureilites, *Meteorit. Planet. Sci.*, *33*, 857–870.